

# Atomistic Quantum Transport Simulation of Topological Insulator $\text{Bi}_2\text{Se}_3$ Tunnel FETs

Jiwon Chang, Leonard F. Register and Sanjay K. Banerjee

Microelectronics Research Center,  
The University of Texas at Austin,  
10100 Burnet Road, Bldg. 160, Austin, TX 78758, U.S.A  
jiwon.chang@utexas.edu

**Abstract**—Three-dimensional (3-D) topological insulators (TI) are characterized by the presence of metallic surface states and a bulk band gap. Recently theoretical and experimental studies have shown an induced gap in the surface state bands of TI thin films. The gap results from interaction of conduction band (CB) and valence band (VB) surface states from the opposite surfaces of a thin film, and its size is determined by the thin film thickness. This gap opening could open the possibility of TI-based MOSFETs and band-to-band tunnel FETs. In this work we consider the latter. Specifically, we explore the transport properties of lateral tunnel FETs based on  $\text{Bi}_2\text{Se}_3$ , one of the most promising TI materials, using quantum ballistic transport simulations with the tight-binding Hamiltonian in the atomic orbital basis.

**Keywords**—component; topological insulator, tunnel FET, atomistic, quantum transport

## I. INTRODUCTION

Three-dimensional (3-D) topological insulators (TIs) have gained substantial interest recently because of their novel electronic surface states [1,2]. A 3-D TI is characterized by the presence of protected spin-polarized semi-metallic surface states with the conduction band (CB) and valence band (VB) meeting at a Dirac point, separated by an insulating bulk, as illustrated in Fig. 1(a). Conducting surface states of TI are quite robust to the nonmagnetic disorder but open a gap in the presence of time-reversal symmetry breaking perturbations [3]. However, recent theoretical and experimental studies have shown an induced gap within the surface bands in TI thin films even without magnetic disorders [4,5]. The gap originates from allowed VB-to-CB surface states interactions between the opposite surfaces as shown in Fig. 1(b), with a gap size determined by the thin film thickness. (CB-to-CB and VB-to-

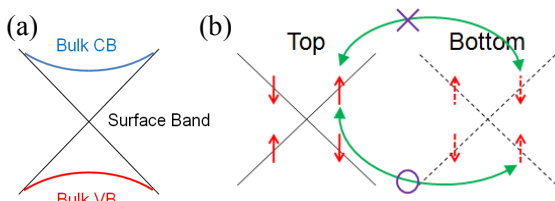


Figure 1. (a) Schematic view of TI band structure. Surface bands reside within a bulk band gap. (b) Schematic description of the interaction between surface states on opposite surfaces of a thin film. Due to the spin polarized property of surface states, the CB to VB interaction (only) is allowed.

VB inter-surface interactions are essentially forbidden by their orthogonal spin status.) This gap opening allows for the possibility of TI-based band-to-band Tunnel FETs (TFETs). In this work, we use atomistic tight-binding (TB) based nonequilibrium Green's function (NEGF) simulations with TB potentials obtained from density functional theory (DFT), to explore the possibility of band-to-band TFETs based on thin film TIs. Primarily, we consider tunneling parallel to the surfaces within a p-i-n (source/gated-channel/drain) structure common for many TFET designs, in  $\text{Bi}_2\text{Se}_3$  which is one of the most promising TI materials. TI-based TFETs would be analogous in some ways to proposed graphene nanoribbon TFETs, but without the sensitivity to ribbon width and edge roughness, and in some ways to narrow gap III-V TFETs but with substantially thinner quantum well widths.

## II. SURFACE BAND STRUCTURES OF $\text{Bi}_2\text{Se}_3$ THIN FILMS

The primitive unit cell of bulk  $\text{Bi}_2\text{Se}_3$  is rhombohedral with five atoms (two Bi and three Se atoms). Fig. 2(a) shows a cartoon of bulk rhombohedral structure. The three-fold rotation axis is taken along the  $z$ -axis. One can construct a hexagonal unit cell from the rhombohedral cell with the lattice parameters  $a=0.4138$  nm and  $c=2.8633$  nm (Fig. 2(a), the larger cell). The building block of the hexagonal bulk  $\text{Bi}_2\text{Se}_3$  crystal consists of five atomic layers referred to as quintuple layer (QL). The square shaded region in Fig. 2(a) shows one such QL.; the entire structure of Fig. 2(a) contains three QLs., i.e., 15 atomic layers stacked along the  $z$ -direction. The atomic planes within a

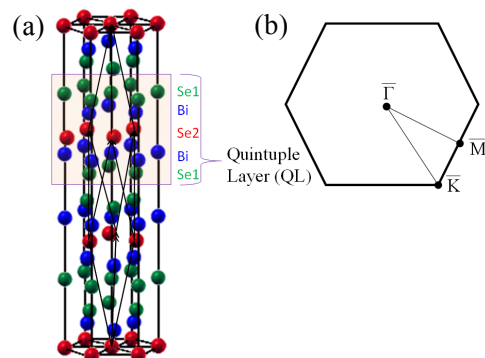


Figure 2. (a) Hexagonal crystal structure of bulk  $\text{Bi}_2\text{Se}_3$ . (b) Two-dimensional hexagonal Brillouin Zone (BZ) of the (111) surface of a  $\text{Bi}_2\text{Se}_3$  thin film.

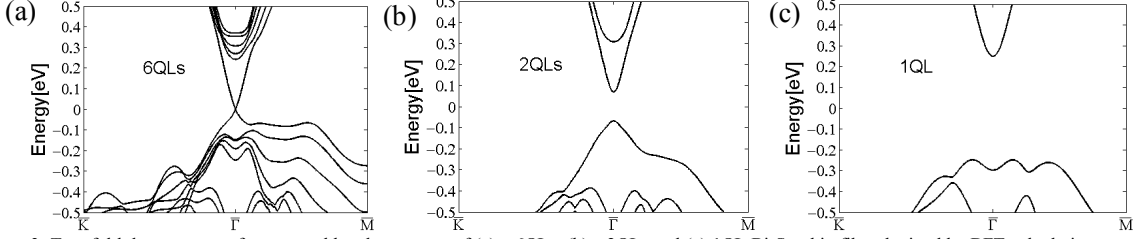


Figure 3. Two-fold degenerate surface-normal band structures of (a) a 6QLs, (b) a 2QLs and (c) 1QL  $\text{Bi}_2\text{Se}_3$  thin film obtained by DFT calculations.

QL are arranged in a sequence Se1-Bi-Se2-Bi-Se1 where the “1” and “2” indicated different Se layer structures. A thin film structure can be formed from one up to a stack of several QLs.

Surface band structures for 6QLs, 2QLs and 1QL  $\text{Bi}_2\text{Se}_3$  thin films are shown in Fig. 3. Band structures are obtained from DFT calculations using the OPENMX code [6], based on a linear combination of pseudoatomic orbital (PAO) method. The pseudopotentials were generated from full relativistic calculations, and the generalized gradient approximation was applied for the exchange-correlation potential [7]. As per the discussion in the introduction, metallic surface states within a bulk band gap ( $\sim 300$  meV) exist in the 6QLs thin film in Fig. 3(a). However, a non-zero gap is produced in 2QLs and 1QL thin films by interactions between CB and VB states from nominally opposite surfaces, while the lack of CB-to-CB and VB-to-VB interactions leaves these surface-state bands two-fold degenerate.

### III. COMPUTATIONAL APPROACH

For the transport calculation, we define a series of rectangular unit cells in the simulation region oriented perpendicular to the transport direction  $x$ , as shown Fig. 4(a) in the top view of a thin film. Three different symbols ( $\circ$ ,  $\square$  and  $\times$ ) are for atomic positions in the different atomic layers stacked in  $z$ -direction. The thin-film 2-D band structure and the

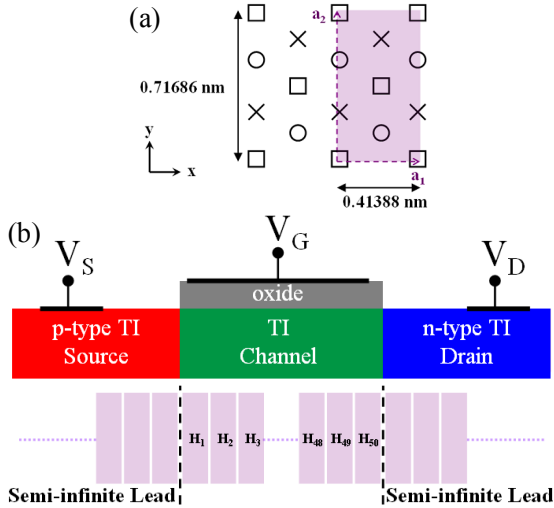


Figure 4. (a) Top view of  $\text{Bi}_2\text{Se}_3$  thin film. A Rectangular unit cell is denoted. (b) Schematic structure of TI thin film TFET composed of a series of rectangular unit cells.

tight-binding (TB) hopping potentials used in the transport calculations are extracted from DFT using maximally localized Wannier functions (MLWFs) [8]. At least 3rd nearest neighbor coupling is used to accurately reproduce the DFT-obtained band structure. Fig. 4(b) shows the layout of the simulated  $\text{Bi}_2\text{Se}_3$  TFETs, with a semi-infinite p-type source, approximately 20 nm long undoped gated channels, and a semi-infinite n-type drain. Probability density is injected into the simulation region from the set of incident propagating eigenmodes of both semi-infinite leads, weighted by the Fermi distribution function of the injecting lead. We use recursive scattering matrices to propagate injected probability from the source (drain), through the channel, to the drain (source), and/or to reflect it back to the source (drain) [9]. The total current is calculated by integrating the injected current over in-thin-film-plane wave-vector components  $k_x$  and  $k_y$ .

We have considered 1QL ( $\sim 0.7$  nm) and 2QLs ( $\sim 1.6$  nm) TI thin film TFETs. Fig. 5(a) and 5(b) show the one-dimensional band structures for the 1QL and 2QLs films, respectively, for transverse modes of  $k_y=0$ , where the band gap minimum occurs at the  $\Gamma$  point—which also would be the Dirac point in thicker structure—and  $k_y=\pi/a_2$  which is the edge of the BZ. The band gaps are 497 and 136 meV for the 1 and 2 QLs thin films,

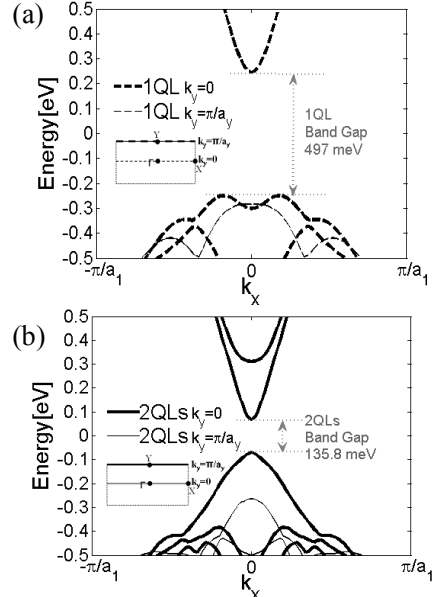


Figure 5. Band structures of (a) 1QL and (b) 2QLs thin films calculated from the TB Hamiltonian at two different transverse modes ( $k_y=0$  and  $\pi/a_2$ ) in the rectangular BZ.

respectively.

#### IV. RESULTS

At the time of writing, these simulations are not electrostatically self-consistent, nor do we assume specific approaches to doping, chemical or electrostatic, or gating. Rather we consider channel potential shifts and pre-defined transition region lengths between the source and channel and channel and drain regions. Two different transition region lengths, about 2.1 nm and 4.1 nm, are considered. With positive drain bias, the gating of the intrinsic channel region controls current flow via overlap (ON) or not (OFF) of the channel CB (VB) with the source VB (drain CB). Under these simulation conditions, we find that the larger band gap 1QL film provides more favorable behavior, with a far below 60 mV/decade subthreshold slope and large ON/OFF ratio in these 300 K ballistic simulations, and a still potentially approaching MOSFET-like transconductance above threshold, as shown in Fig. 6(a) for three different drain biases. The Fermi level in the source (drain) are placed about 8 meV below (above) the CB (VB) edge, corresponding to a charge density of  $2.47 \times 10^{12}/\text{cm}^2$  ( $9.47 \times 10^{13}/\text{cm}^2$ ), to suppress the OFF-state non-tunneling current. The current at three different drain biases (0.3, 0.4 and 0.5 V) with changing the channel potential are plotted in Fig. 6(a). Fig. 6(b) and 6(c) shows the band edge profiles for different potential shifts with  $V_{DS}=0.3$  V, and the corresponding transmission probabilities, respectively. With a 0 eV potential shift (red circle 1 in Fig. 6(a) and red lines in Fig. 6(b)), we have CB-to-VB overlap on the drain side allowing ON-state tunneling. Applying a 0.1 eV potential shift (green circle 2 in Fig. 6(a) and green lines in Fig. 6(b)) pushes down the entire band and removes the CB-to-VB overlap on drain side, thereby leading to negligible current level in Fig. 6(a). With still more potential shift (blue and light blue circle 3 and 4 in Fig. 6(a) and blue and light blue lines in Fig. 6(b)), the CB-to-VB overlap occurs on the source, turning the device back ON. We tested the 2QLs TI film with the Fermi levels in the source and drain in the same position relative to the band edges as for the 1QL device. We calculated the current at  $V_{DS} = 0.05, 0.1, \text{ and } 0.2$  V, respectively. Due to the smaller band gap ( $\sim 136$  meV), even if the Fermi level is very close to the VB (CB) in the source (drain), there is a significant amount of electrons (holes) in CB (VB) of the source (drain). These carriers are the source of the high level of non-tunneling OFF-state current, limiting the ON/OFF ratio to about 10–100 depending on drain bias.

The above simulations, however, were performed with an assumption of about 2.1 and 4.1 nm for the transition lengths, as obtainable in the conventional materials. We performed the self-consistent simulation to estimate the transition region length in  $\text{Bi}_2\text{Se}_3$  thin film. The layout of simulated structure is illustrated in Fig. 7(a). An undoped 1QL thin film is in the middle with  $\text{SiO}_2$  on both sides. We have the gate and drain regions on left and right, respectively. In this structure, we use a direct gating on the drain side. For the test, we applied 0.7 V and  $-0.7$  V on gate and drain regions (which one can think of at least partly as being supplied via work function differences), respectively, to make the corresponding regions n-type and p-type, respectively. The converged potential profile is shown in Fig. 7(b). Even with the direct gating, the transition region is long ( $\sim 16$  nm) due to the high relative dielectric constant of

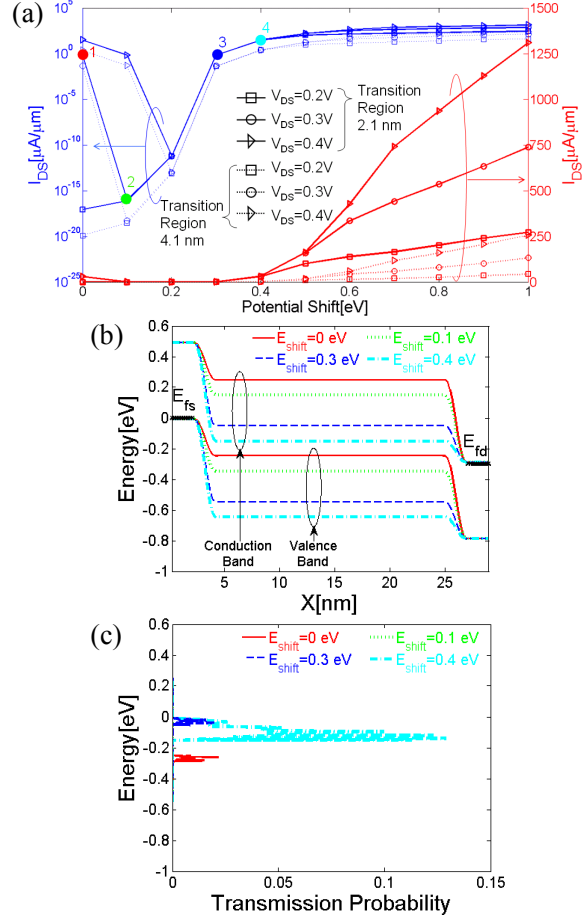


Figure 6. (a)  $I_{DS}$  vs channel potential for two different transition region lengths (about 2.1 and 4.1 nm) at different  $V_{DS}$  in the 1QL thin film device. (b) CB and VB edge profiles and (c) transmission probability plots of the transverse mode at  $k_x=0$  for different potential shifts at  $V_{DS}=0.3$  V in the 1QL thin film device with the transition region length of about 2.1 nm.

$\text{Bi}_2\text{Se}_3$  ( $\sim 100$ ) [10]. The extremely high dielectric constant proves problematic for creating a rapid potential variation along the channel which is essential to achieve the high ON current.

Going forward we will be considering two options, the use of lower dielectric constant TIs, such as  $\text{TlBiSe}_2$  with a dielectric constant of 25 that is comparable to conventional high-k dielectrics such as hafnium-oxide, and an alternative TFET geometry where a large TI dielectric permittivity should prove advantageous. In the latter case, as illustrated in Fig. 8(a), there are two TI thin films with a conventional insulator in between acting as a tunnel barrier. If we apply an electric field perpendicular to the thin film, most of the potential is dropped in the barrier layer due to very high dielectric constant of the TIs, leading to an abrupt potential change between the adjacent sides of the two TI thin films. Fig. 8(b) and (c) are the surface normal band structures for a system of two 1QL  $\text{Bi}_2\text{Se}_3$  thin films separated by a monolayer of BN without and with an electric field, respectively, obtained by DFT calculations.

Applying an electric field induces shifting of surface bands on different  $\text{Bi}_2\text{Se}_3$  films. In Fig. 8(c) at the crossing points between CB of the top  $\text{Bi}_2\text{Se}_3$  and the VB of the bottom  $\text{Bi}_2\text{Se}_3$  layer, there exist anti-crossing gaps indicating the coupling between the  $\text{Bi}_2\text{Se}_3$  thin films by which gated interlayer tunneling could occur.

## V. CONCLUSION

We performed quantum ballistic transport simulations using a tight-binding Hamiltonian in the atomic orbital basis to assess the feasibility of  $\text{Bi}_2\text{Se}_3$  for TFET applications. Two different thickness thin films of  $\text{Bi}_2\text{Se}_3$ , 1QL ( $\sim 0.7$  nm) and 2QLs ( $\sim 1.6$  nm) whose gap sizes are about 0.5 and 0.13 eV, respectively, are considered. Base on ON/OFF ratio, the 1QL  $\text{Bi}_2\text{Se}_3$  shows the better device performance than 2QLs due to its larger band gap. However, the limited tunnel barrier thickness obtainable with in conventional material systems and associated substantial transconductances associated with tunnel barrier thickness seem unlikely to survive into the TI system because of the electrostatics associated with the extremely large dielectric constant. We have begun exploring surface-normal tunneling in a TI bilayer structure with a middle insulating layer where the high dielectric constant can be turned to advantage.

## ACKNOWLEDGMENT

The authors acknowledge financial support from the Nanoelectronics Research Initiative supported Southwest Academy of Nanoelectronics (NRI-SWAN) center. We thank the Texas advanced computing center (TACC) for computational support.

## REFERENCES

- [1] M. Z. Hasan and C. L. Kane, "Colloquium: Topological insulators," *Rev. Mod. Phys.*, vol 82, pp. 3045-3067, 2010.

- [2] J. E. Moore, "The birth of topological insulators," *Nature*, vol. 464, pp. 194-198, 2011.
- [3] Q. Liu, C. X. Liu, C. Xu, X. L. Qi, and S. C. Zhang, "Magnetic impurities on the surface of a topological insulator," *Phys. Rev. Lett.*, vol. 102, no. 156603, 2009.
- [4] Y. Zhang *et al.*, "Crossover of the three-dimensional topological insulator  $\text{Bi}_2\text{Se}_3$  to the two-dimensional limit," *Nature Physics*, vol. 6, pp. 584-588, 2010.
- [5] J. Chang, L. F. Register, S. K. Banerjee and B. Sahu, "Density functional study of ternary topological insulator thin films," *Phys. Rev. B*, vol 83, no. 235108, 2011.
- [6] T. Ozaki and H. Kino, "Efficient projector expansion for the ab initio LCAO method," *Phys. Rev. B*, vol. 72, no. 045121, 2005.
- [7] J. P. Perdew, K. Burke and M. Ernzerhof, "Generalized Gradient Approximation Made Simple," *Phys. Rev. Lett.*, vol. 77, pp. 3865-3868, 1996.
- [8] H. Weng, T. Ozaki, and K. Terakura, "Revisiting magnetic coupling in transition-metal-benzene complexes with maximally localized Wannier functions," *Phys. Rev. B*, vol. 79, no. 235118, 2009.
- [9] T. Usuki, M. Saito, M. Takatsu, R. A. Kiehl, and N. Yokoyama, "Numerical analysis of ballistic-electron transport in magnetic fields by using a quantum point contact and a quantum wire," *Phys. Rev. B*, vol. 52, pp. 8244-8255, 1995.
- [10] H. Kohler and C. R. Becker, "Optically active lattice vibrations in  $\text{Bi}_2\text{Se}_3$ ," *Physica status solidi (b)*, vol. 61, pp. 533-537, 1974.

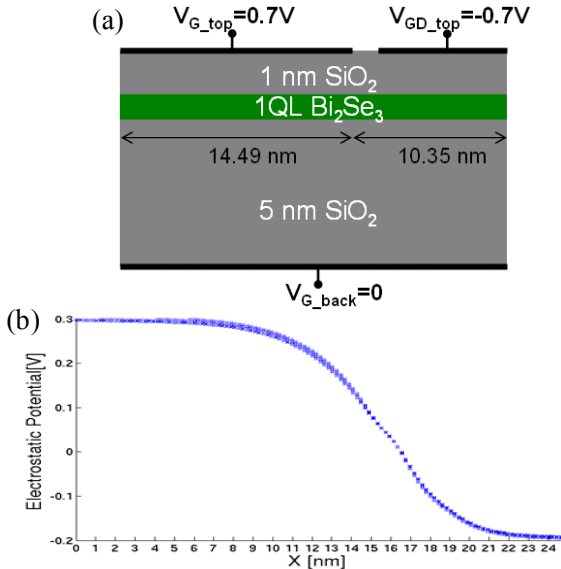


Figure 7. (a) Schematic structure in the self-consistent calculation for estimating the transition length. (b) Converged potential profile.

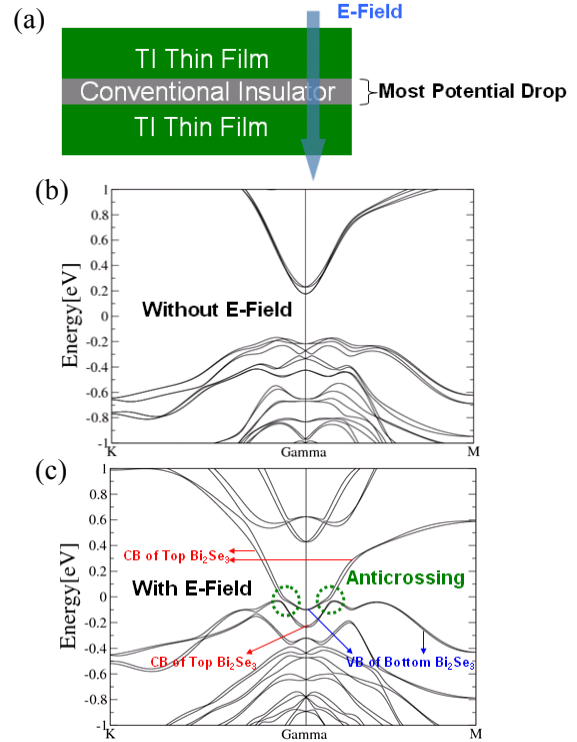


Figure 8. (a) TI thin film bilayer structure with a (more) conventional insulating layer in the middle. Band structures of two 1 QL  $\text{Bi}_2\text{Se}_3$  thin films sandwiching a layer of BN in between (b) without and (c) with the electric field. Note within (c) that the potential is predominately dropped between the two  $\text{Bi}_2\text{Se}_3$  layers, and that there is an anti-crossing between the CB of the top TI layer and the VB of bottom TI layer, indicating the inter-TI-layer coupling by which gated interlayer tunneling could occur.